

Local convertibility and edge states in quantum many body systems

Fabio Franchini,^{1,2,*} Jian Cui,^{3,4} Luigi Amico,^{5,6} Heng Fan,³ Mile Gu,^{6,7} Vladimir E. Korepin,⁸ Leong Chuan Kwek,^{6,9} and Vlatko Vedral^{10,6}

¹Department of Physics, Massachusetts Institute of Technology, Cambridge, MA 02139, U.S.A.

²SISSA and I.N.F.N, Via Bonomea 265, 34136, Trieste, Italy

³Institute of Physics, Chinese Academy of Sciences, Beijing 100190, China

⁴Freiburg Institute for Advanced Studies, Albert Ludwigs University of Freiburg, Albertstrae 19, 79104 Freiburg, Germany

⁵CNR-MATIS-IMM & Dipartimento di Fisica e Astronomia, Via S. Soa 64, 95127 Catania, Italy

⁶Centre for Quantum Technologies, National University of Singapore, 3 Science Drive 2, Singapore 117543

⁷Center for Quantum Information, Institute for Interdisciplinary Information Sciences, Tsinghua University, Beijing, China

⁸C. N. Yang Institute for Theoretical Physics, Stony Brook University, NY 11794, USA

⁹National Institute of Education and Institute of Advanced Studies,

Nanyang Technological University, 1 Nanyang Walk, Singapore 637616

¹⁰Atomic and Laser Physics, Clarendon Laboratory, University of Oxford, Parks Road, Oxford, OX13PU, United Kingdom

Certain entanglement (Renyi) entropies of the ground state of an extended system can increase even as one moves away from quantum states with long range correlations. In this work we demonstrate that such a phenomenon, known as non-local convertibility, is due to the edge state (de)construction occurring in the system. To this end, we employ the example of the ground state of the “2-SAT”/Ising model, displaying an order-disorder quantum phase transition. We consider both the thermal ground state, enjoying the same symmetry of the Hamiltonian, and the ferromagnetic ground state with a non vanishing local order parameter. Employing both analytical and numerical methods, we compute entanglement entropies for various system’s bipartitions ($A|B$). We find that the ground states enjoying the Hamiltonian symmetries show non-local convertibility if either A or B are smaller than, or of the order of, the correlation length. A ferromagnetic ground state, instead, is always locally convertible. Our interpretation in terms of the edge states behavior explains all these results and could disclose a paradigm to study the local convertibility protocol in both topologically ordered and topologically trivial quantum phases, in a unified way and provides a clear characterization of which features a *universal quantum simulator* should possess to outperform a classical machine.

Introduction.— Quantum many-particle systems can exhibit collective phenomena that are inconceivable for their classical counterparts. This has motivated analysis that combine ideas and techniques of diverse fields including quantum optics, quantum information, and condensed matter physics. Such ‘cultural osmosis’ has dramatically enriched our understanding of quantum effects. Quantum statistical mechanics, for example, revealed that quantum phases of matter can be understood in terms of non-local quantum correlations, entanglement entropies being a popular example [1–3]. These quantum correlations constitute a recognized portent in emerging quantum technology [4]. Adiabatic quantum computation is an important example: a quantum information processing protocol, whose computational power is influenced by an order-disorder transition [5].

Although quantum coherence is clearly important for quantum information processing [6–8], it is of the same importance to understand to what extent the coherent manipulation is indeed a defining property of the algorithm. In this context, the adiabatic quantum computing algorithm of the “2-SAT”/Ising model was recently reconsidered, partitioning a *finite, closed system* into two subsystems, A and B , process we indicate as ($A|B$). It was argued in [9] that coherent non-local operations between A and B are necessary to simulate the adiabatic quantum evolution within the ordered phase; whereas bipartite local methods (within A and B , respectively) are sufficient in the disordered region, with this sudden change in the ability to perform the computation locally occurring at the finite-

size scaling point of the Hamiltonian (i.e. yielding a quantum phase transition in the thermodynamic limit). Similar lack of *local convertibility* has been observed also for the ground states of certain models showing topological order [10, 11].

In this work we provide an explanation for this phenomenon, in terms of localized states that the system is able to create at its boundaries (edge states). To this end, we investigate the local convertibility of the Ising/2-Sat model for an *infinitely large* system. Employing a combination of analytical and numerical techniques, we explore the role of the A and B block sizes with respect to the correlation length of the system. An important aspect of the problem we consider is provided by the symmetry-breaking mechanism, the study of which helps us in characterizing the role of the boundary states. Our findings indicate that models with edge modes show intrinsic greater computational power than any classical simulator.

Local convertibility and Renyi entropies.— One key property of entanglement measures is that they do not increase under local quantum operations and classical communication (LOCC). Considering pure bipartite quantum states, take, for instance, the two states

$$\begin{aligned} |\psi_1\rangle &= \sqrt{0.4}|11\rangle + \sqrt{0.4}|22\rangle + \sqrt{0.1}|33\rangle + \sqrt{0.1}|44\rangle, \\ |\phi_1\rangle &= \sqrt{0.5}|11\rangle + \sqrt{0.25}|22\rangle + \sqrt{0.25}|33\rangle. \end{aligned} \quad (1)$$

While it is not possible to convert $|\phi_1\rangle$ into $|\psi_1\rangle$ by LOCC, it is possible to operate locally on $|\psi_1\rangle$ to transform it into $|\phi_1\rangle$, if assisted by the ancillary entangled state $|a\rangle = 0.6|00\rangle + 0.4|11\rangle$

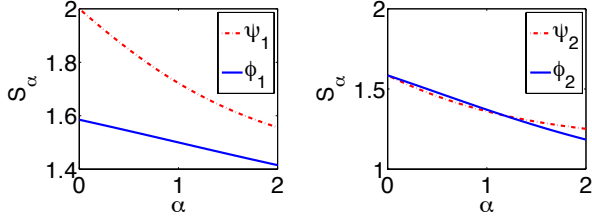


FIG. 1. (Color online) Plot of the entanglement Renyi entropies of two bipartite states $|\psi\rangle$ and $|\phi\rangle$ may characterize two types of behavior: if the entropy curves do not touch each other, $|\psi_2\rangle$ can be locally converted to $|\phi_2\rangle$, see (1); if the two curves intersect (left), the two states, like those in (2), cannot be locally transferred to each other.

[13]. If, instead, we take the two quantum states

$$\begin{aligned} |\psi_2\rangle &= \sqrt{0.5}|11\rangle + \sqrt{0.4}|22\rangle + \sqrt{0.1}|33\rangle, \\ |\phi_2\rangle &= \sqrt{0.6}|11\rangle + \sqrt{0.2}|22\rangle + \sqrt{0.2}|33\rangle, \end{aligned} \quad (2)$$

it can be shown that they cannot to be converted into each other by LOCC [12], even with aids from ancillas. These properties can be captured through the entanglement Renyi entropies $S_\alpha(\rho_A) \equiv \frac{1}{1-\alpha} \log_2[\text{Tr} \rho_A^\alpha]$ of the reduced density operator of subsystem A : The necessary and sufficient condition for $|\phi\rangle$ to be locally convertible to $|\psi\rangle$ is that the inequality holds $S_\alpha(|\psi\rangle) \geq S_\alpha(|\phi\rangle)$ for all α [14]. In this case, state $|\psi_{AB}\rangle$ can be converted locally to another state $|\phi_{AB}\rangle$ of lower entanglement, possibly assisted by a “catalyst” state. The above examples can be understood clearly by looking at their entanglement Renyi entropies, as show in Fig. 1.

The notion of differential local convertibility was first discussed in a many-body scenario in Ref. [9]. Accordingly, let $|GS(g)\rangle$ be the ground state of a given Hamiltonian $H(g)$, depending on a control parameter g . As g is varied, it is questioned whether the adiabatic evolution of $|GS(g)\rangle$ into the ground state of $H(g+\delta)$, $|GS(g+\delta)\rangle$, can be simulated through assisted LOCC in A and B (bi-partitioning the system as explained in the introduction). As explained above, the answer to this question lies in the majorization condition on the Renyi entropies, which is equivalent to $\partial_g S_\alpha(g) \leq 0$ (or $\partial_g S_\alpha \geq 0$), $\forall \alpha$: this property is thus called *differential convertibility*. Besides its own interest, it would be important to understand the interplay between convertibility protocols and the adiabatic quantum computation. As we shall see, our analysis opens the way to make a precise contact between the two notions.

The “2-SAT” problem.— In computing science, many interesting tasks can be recast into equivalent problems of finding some N variable assignments that minimize certain “energy” functions. The problem is written in terms of Boolean clauses, each of which involves the N individual variables, and the minimum energy corresponds to the satisfaction of all these clauses, hence the name the *N-Satisfiability Problem*. For $N > 2$, the general “N-SAT” is NP-complete, which means that there is no known algorithm that efficiently solves all instances of “N-SAT” problems. This has been the first known

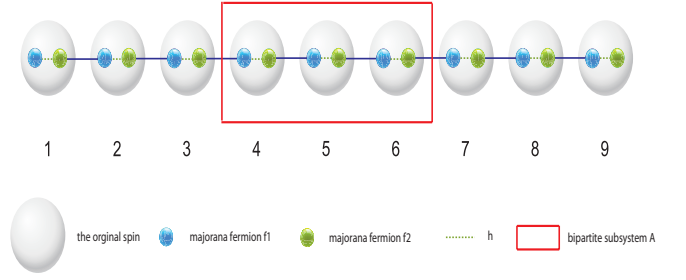


FIG. 2. (Color online) The Ising chain and its Majorana fermions formulation.

example of an NP-complete problem. The “2-SAT”, located at the fundamental level of the “N-SAT” hierarchy, however, is in P problem. Namely there exists classical algorithms that are able to solve it in polynomial time.

The evolution Hamiltonian of the “2-SAT” problem is the transverse field Ising model,

$$H_I = - \sum_{j=1}^N (\sigma_j^x \sigma_{j+1}^x + h \sigma_j^z), \quad (3)$$

where σ_j^α are the Pauli matrices, h is the external magnetic field driving the quantum phase transition (QPT) occurring in the thermodynamic limit of $N \rightarrow \infty$ at $h = 1$. The Hilbert space of (3) can be described in terms of eigenstates of the string operator $\mu_N^x = \prod_{j=1}^N \sigma_j^x$, which generates the \mathbb{Z}_2 symmetry of (3). For $h > 1$ the system is paramagnetic with $\langle \sigma^x \rangle = 0$. For $h < 1$, the spectrum of the Ising model becomes doubly degenerate. The ground state enjoying the same symmetry of the Hamiltonian, known as the ‘thermal ground state’, is thus an eigenstate of μ_N^x and hence has a vanishing order parameter $\langle \sigma_x \rangle = 0$. This is the actual ground state of the 2-Sat problem, usually employed in the adiabatic quantum computation protocols for finite N . In the thermodynamic limit $N \rightarrow \infty$, σ^x can acquire a non-zero expectation value. spontaneously breaking the symmetry, and the ground state is given by the (anti)symmetric combination of the the two eigenstates of μ_N^x . For $h < 1$ we consider both this ferromagnetic ground state and the thermal one with definite \mathbb{Z}_2 parity: we find that only the latter can break local convertibility, while the former shows a monotonous entropy derivative.

The \mathbb{Z}_2 symmetric ground state— The quantum Ising model (3) can be mapped exactly, although non-locally, on a system of free spinless fermions $\{c_j, c_j^\dagger\}$ [16]. Incidentally, we remark that this mapping preserves the entanglement between A and B and generate the so-called *1D Kitaev model* [17]. As discussed in a series of papers [18, 19], for quadratic theories like this, one can extract the entanglement spectrum from the correlation matrix of all 2-point functions. However, the Ising model enjoys an even more powerful formalism, in terms of Majorana fermions $f_j^{(1)} \equiv c_j^\dagger + c_j$, $f_j^{(2)} \equiv i(c_j^\dagger - c_j)$ whose properties were highlighted by Kitaev [17].

We represent this mapping pictorially in figure 2. In the paramagnetic phase ($h > 1$), the Hamiltonian pairs predominantly Majoranas on the same site j (this correlation is drawn

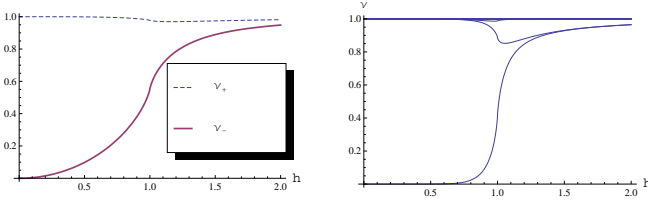


FIG. 3. Plot of the “eigenvalues” ν_j ’s of the correlation matrix (4) as a function of h for $L = 2$ (left) and $L = 10$ (Right). For $L = 2$, the explicit form of the eigenvalues ν_{\pm} is given in (9). Notice that only one of the ν ’s shows a non-trivial behavior: it corresponds to the boundary state, which is only partially contained in the subregion.

as dash line in the picture). In the ferromagnetic phase, the solid line connecting different sites is dominant. In Kitaev’s approach, the double degeneracy of this phase emerges as the first and last Majoranas are left unpaired by the Hamiltonian and can be combined into a complex fermion, whose occupancy/vacancy costs no energy. We will see that the same picture applies when the system is cut into two partitions, since doing so in the ferromagnetic phase cuts the dominant link and leaves unpaired edge states on each side of the cut.

To show this, we employ the thermal ground state that is amenable of exact analytical treatment. The symmetry broken states will be analyzed in the next section within a numerical approach. For the former ground state, the eigenvalues of the reduced density matrix of a block of L consecutive spins can be obtained from the diagonalization of the $2L \times 2L$ correlation matrix [20, 21]: $\langle f_k^{(a)} f_j^{(b)} \rangle = \delta_{j,k} \delta_{a,b} + i (\mathcal{B}_L)^{(a,b)}_{(j,k)}$, with

$$\mathcal{B}_L \equiv \begin{pmatrix} \Pi_0 & \Pi_1 & \dots & \Pi_{L-1} \\ \Pi_{-1} & \Pi_0 & & \vdots \\ \vdots & & \ddots & \vdots \\ \Pi_{1-L} & \dots & \dots & \Pi_0 \end{pmatrix}, \quad (4)$$

where j, k specifies the entry $\Pi_{j-k} \equiv \begin{pmatrix} 0 & g_{j-k} \\ -g_{k-j} & 0 \end{pmatrix}$, which is itself a 2×2 matrix whose a, b entries are defined as

$$g_j \equiv \frac{1}{2\pi} \int_0^{2\pi} \frac{\cos \theta - h + i \sin \theta}{\sqrt{(\cos \theta - h)^2 + \sin^2 \theta}} e^{ij\theta} d\theta. \quad (5)$$

The anti-symmetric matrix \mathcal{B} can be brought into a block-diagonal form by a $SO(2L)$ rotation, with each block of the form $\tilde{\Pi}_j = \nu_j \begin{pmatrix} 0 & 1 \\ -1 & 0 \end{pmatrix}$. This rotation defines a new set of Majorana fermions $\tilde{f}_j^{(a)}$ with only pair-wise correlations. This rotated operator basis can be used to introduce a new set of complex operators: $\tilde{c}_j = (\tilde{f}_j^{(1)} + i\tilde{f}_j^{(2)})/2$ (and its hermitian conjugated); in such a basis the Hamiltonian results diagonal as well. As discussed in [21], the matrix (4) contains all the informations to completely solve the model. By taking $L = N$, i.e. extending the correlation matrix to the whole system, the ground state $|0\rangle$ can be characterized as the one annihilated by all the \tilde{c}_j and the full Fock space is constructed by all possible

applications of the creation operators \tilde{c}_j^\dagger to this vacuum. For $L < N$, one proceeds similarly and defines a different set of $\tilde{c}_j, \tilde{c}_j^\dagger$, which spans a Hilbert space of dimension 2^L .

We observe that the elements of the reduced density matrix ρ_A are indeed the overlaps between the ground state and the different states of the Hilbert space spanned by $\tilde{c}_j, \tilde{c}_j^\dagger$. Because we deal with a quadratic theory, we can characterize each of the block states in terms of its individual excitations. We note that the bilinears $\tilde{c}_j \tilde{c}_j^\dagger$ and $\tilde{c}_j^\dagger \tilde{c}_j$ act as projection operators on states with the j -th excitation empty or occupied. Therefore, the expectation values

$$\langle 0 | \tilde{c}_j \tilde{c}_j^\dagger | 0 \rangle = \frac{1 + \nu_j}{2}, \quad \langle 0 | \tilde{c}_j^\dagger \tilde{c}_j | 0 \rangle = \frac{1 - \nu_j}{2}, \quad (6)$$

are indeed the building blocks of the Schmidt bipartite decomposition of the ground state [22]. It is worth noting that an “eigenvalue” ν_j close to unity indicates that \tilde{c}_j annihilates the vacuum $|0\rangle$ and thus that a quasi-particle excitation of the Hamiltonian is completely contained in the block. As exploited in [20, 21], using (6), the L “eigenvalues” ν_j ’s of \mathcal{B}_L can be used to construct the 2^L eigenvalues λ_l of the reduced density matrix ρ_A as

$$\{\lambda_l\} = \prod_{j=1}^L \left(\frac{1 \pm \nu_j}{2} \right), \quad (7)$$

with all the possible combinations of plus/minus signs, corresponding to the occupation/unoccupation of the different excitations of \mathcal{B}_L . The Renyi entropies are given as

$$S_\alpha(\rho_A) = \frac{1}{1-\alpha} \sum_{j=1}^L \log \left[\left(\frac{1 + \nu_j}{2} \right)^\alpha + \left(\frac{1 - \nu_j}{2} \right)^\alpha \right]. \quad (8)$$

In figure 3 we plot the correlation matrix “eigenvalues” ν_j ’s as a function of the magnetic field for $L = 2$ and $L = 10$. We notice that in both cases only one mode has a non trivial behavior, while the other eigenvalues stay approximately constant around unity (with significant deviations only close to the QPT, as the correlation length diverges). In the sense specified above, these modes with $\nu_j \simeq 1$ defines the *bulk states*. In contrast, the non-trivial eigenvalue ν_0 is close to zero for $h < 1$; correspondingly, only half of the fermionic excitation is present in the spin-block (6): as we anticipated, *by cutting the chain into two subregions, we severed the dominant inter-site correlation and hence generated two unpaired Majorana edge states*.

Now that we discussed the behavior of the eigenvalues of \mathcal{B}_L and the role of the boundary states, we proceed to analyze the Renyi entropies and the issue of differential local convertibility. We present the results for the two extreme limits: $L = 2$ and $L \rightarrow \infty$.

In terms of (5), the two eigenvalues of the correlation matrix for $L = 2$ are found to be

$$\nu_{\pm} = \sqrt{\left(\frac{g_1 - g_{-1}}{2} \right)^2 + g_0^2} \pm \frac{g_1 + g_{-1}}{2}, \quad (9)$$

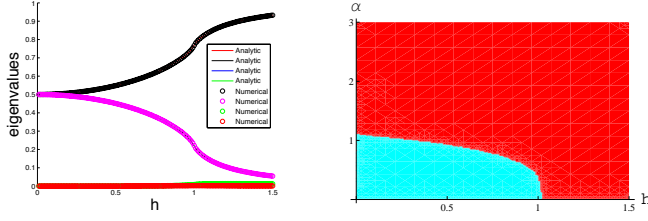


FIG. 4. (Color online) Left: Plot of the four eigenvalues of ρ_A for $L = 2$, as a function of h . The solid lines are the analytical results and the circles show the numerical ones with $N=200$

. Right: Contour plot of the sign of the derivative by h of the Renyi entropy for different values of h and α .

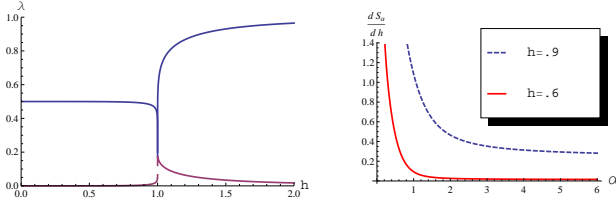


FIG. 5. Left: Plot of the first few eigenvalues of ρ_A for an infinite size subregion, as a function of h , multiplicities not shown (for instance, the highest eigenvalue is doubly degenerate for $h < 1$ and unique for $h > 1$, see [25]). Right: Plot of the derivative of the Renyi entropy with respect to the magnetic field h , as a function of α , for two different values of h in the ferromagnetic region.

which allows for a complete analytical study of the entanglement entropy and its derivative. These eigenvalues are shown in the left plot of Fig. 3. In Fig. 4, we plot the resulting four eigenvalues of the reduced density matrix according to (7) and the sign of the entanglement entropy derivative that we calculate from (8) using (9). We see that, while in the paramagnetic phase the Renyi entropy is always decreasing, in the doubly degenerate phase the entropy derivative vanishes at some value of α and changes sign, indicating that local (differential) convertibility is lost in this phase, as already observed numerically (for small N) in [9].

For the $L \rightarrow \infty$ limit, we can use the results of [23–25], where the full spectrum (eigenvalues and multiplicities) of the reduced density matrix and the Renyi entropies were calculated analytically. Fig. 5 shows a plot of the first few eigenvalues of ρ_A and a plot of the entropy derivative as a function of α for $h = 0.6$ and $h = 0.9$. It is clear that the Renyi entropy is monotonous and that local convertibility is restored in the infinite size limit.

We check these results, by performing numerical calculations with system sizes up to $N = 200$ and with different partitions, both by considering different block sizes and by moving the blocks within the chain. The qualitative picture does not change significantly as one varies $(A|B)$, but the location of the curve where the entropy derivative vanishes moves in (h, α) space and tend to approach the phase transition line $h = 1$ as the block sizes grow bigger than any length scale in the system, confirming our expectation on the role of the

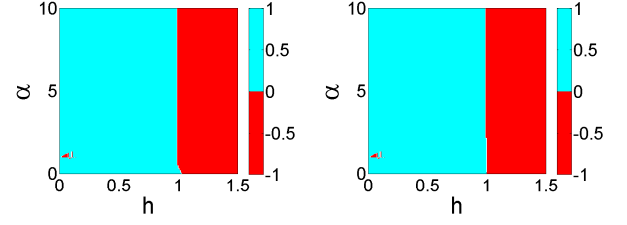


FIG. 6. (Color online) Numeric results of differential local convertibility for the ferromagnetic (symmetry broken). On the left, a partition $200 = 2|198$, on the right $200 = 50|100|50$.

boundary excitations. Namely, we see that as long as the edge states from different boundaries do not overlap, their “eigenvalue” ν_0 stays constant and vanishing and starts increasing only once the correlation length grow comparable to one of the block sizes, indicating edge states recombination.

Symmetry broken ground state—To further confirm our interpretation on the role of boundary modes, in the ordered phase $h < 1$ we also considered the ferromagnetic ground state for which $\langle \sigma^x \rangle \neq 0$. Since this state does not support well defined Majorana edge states, we expect a restoration of local convertibility. We calculate the Renyi entropies of this symmetry broken ground state numerically. Namely we add a very small perturbation $\epsilon(\sigma_1^x + \sigma_N^x)$ to Hamiltonian (3) and apply it to the variational MPS routine to obtain the ground state. In this work the converge tolerance is 10^{-6} . Fig. 6 shows the plots of the sign of the derivative entropy for two possible partitions (small and large A block) and validates our expectation that both phases are locally convertible. We considered several partitioning choices and the results are not distinguishable from those in fig. 6.

Conclusions and discussions—In this work we studied the differential local convertibility in the paradigmatic order-disorder quantum phase transition occurring by varying the control parameter h in the quantum Ising model/2-SAT problem. While the disordered ground state $h > 1$ results always locally convertible, a complex scenario emerges for the phase with $h < 1$. For the thermal ground state, enjoying the same symmetry of the Hamiltonian, the convertibility depends on the interplay between the size of the partition $(A|B)$ and the correlation length of the system. For the ferromagnetic ground state, i.e. with broken symmetry, the local convertibility is restored, for any chosen partition.

We identified the edge states forming at the partition boundaries as the relevant degrees of freedom controlling the local convertibility of the ground state: *when the correlation length becomes of the order of one of the subregions, the edge states at opposite boundaries can combine to form nearly bulk states. By further increasing of the correlation length, the reduced density matrix eigenvalue corresponding to the overlap between bulk and boundary modes can increase and this implies that the large- α Renyi entropies can decrease (while low- α entropies increase, because more states are required to construct the reduced density matrix in the Schmidt decomposi-*

tion), yielding a non-local convertibility. In contrast, for block sizes remaining larger than the correlation length, the edge states of different boundaries cannot recombine and the two degenerate block states do not split. In this way, an (approximately) flat entanglement spectrum is established to satisfy the sum rule $\sum \lambda_l = 1$. Accordingly, all the Renyi entropies are monotonous, implying that the local convertibility is restored. We note that the edge states are washed out in the symmetry broken case, and therefore the observed monotonous behavior of the Renyi entropies follow from the considerations above. It would be interesting to confirm analytically these expectations.

We believe that the scenario we discussed can be useful in various fields, including condensed matter physics and adiabatic quantum computation. Since the reduced density matrix eigenvalues are a reflection of the spatial distribution of the quasi-particle excitations, we believe that something similar to our edge-formation-mechanism is at play in different quantum phases of matter, including the topological models, recently proved to be non local convertible[10, 11]. One way to check the validity of our picture is to consider (artificial) superpositions of the degenerate ground states. Such superposition can be in principle realized through the application of a non-local perturbation (i.e. a string operator) and should give rise to a local convertible state.

Finally, we observe that lack of differential local convertibility for very small partitions (already $L = 2$) indicates that local classical gates are less efficient than a quantum algorithm in simulating an adiabatic evolution even while moving away from a critical point. In fact, while in quantum protocols locality is defined in terms of the two partitions, which could even be macroscopic, realistic implementations of classical protocols are constructed out of 2-bit operations and thus this is the level of locality to be considered in comparing quantum and classical algorithms. Hence, we demonstrated that non-local convertible phases offer a computational advantage to quantum algorithms compared to classical ones and thus satisfy a necessary criterion for the construction of a “universal quantum simulator”, as discussed by Feynman in his seminal paper [26].

An interesting extension of the present work is to consider the XY chain and its local convertibility under different partitions. These directions for future works are currently under investigation and we shall report on them in the near future.

Acknowledgment– We thank Alioscia Hama for several fruitful discussions. F.F. thanks Chen Fang for his interesting seminar and his insights. FF was supported by a Marie Curie International Outgoing Fellowship within the 7th European Community Framework Programme (FP7/2007-2013) under the grant PEOF-PHY-276093. J.C. acknowledges MPG RZ Garching for the computational resource. HF is supported by 973 program (2010CB922904) and grants from NSFC and CAS. M.G., L.C.K., and V.V. are supported by the National Research Foundation & Ministry of Education, Singapore. M.G. is also supported by National Basic Research Program of China Grant 2011CBA00300, 2011CBA00302, the Na-

tional Natural Science Foundation of China Grant 61033001, 61061130540.

Supplementary material

Finite subsystem

For $L = 2$, the “eigenvalues” of the correlation matrix \mathcal{B}_L in eq. (4) can be found to be those of eq. (9). The Renyi entropy is thus

$$S_\alpha = \frac{1}{1-\alpha} \sum_{\sigma=\pm} \ln \left[\left(\frac{1+\nu_\sigma}{2} \right)^\alpha + \left(\frac{1-\nu_\sigma}{2} \right)^\alpha \right]. \quad (10)$$

and its derivative is

$$dS_\alpha = \frac{\alpha}{1-\alpha} \sum_{\sigma=\pm} \frac{(1+\nu_\sigma)^{\alpha-1} - (1-\nu_\sigma)^{\alpha-1}}{(1+\nu_\sigma)^\alpha + (1-\nu_\sigma)^\alpha} d\nu_\sigma. \quad (11)$$

Note that the asymptotic behaviors of the entropy derivative are given by:

$$\lim_{\alpha \rightarrow 0} \frac{dS_\alpha}{d\alpha} = - \sum_{\sigma=\pm} \frac{\nu_\sigma}{1-\nu_\sigma^2} d\nu_\sigma, \quad (12)$$

$$\lim_{\alpha \rightarrow \infty} dS_\alpha = - \sum_{\sigma=\pm} \frac{1}{1+\nu_\sigma} d\nu_\sigma, \quad (13)$$

and it is easy to see that in the ferromagnetic phase these two limits have opposite signs, indicating lack of local convertibility. The right-hand side of fig. 4 in the paper shows a plot of the sign of eq. (11). The derivatives $\frac{d\nu_\sigma}{dh}$ are calculated analytically from the definitions of the coefficients of the correlation matrix, eq. (5): although all the quantities appearing in (11) are a combination of elementary functions and complete elliptic integrals, in the plot the latter were evaluated numerically directly from the expression given.

For higher L , we obtained the “eigenvalues” ν_l from the numerical diagonalization of the $L \times L$ Hankel matrix:

$$\tilde{\mathcal{B}} = \begin{pmatrix} g_{L-1} & g_{L-2} & \cdots & g_0 \\ g_{L-2} & g_{L-3} & \cdots & g_{-1} \\ \vdots & & \ddots & \vdots \\ g_0 & g_{-1} & \cdots & g_{1-L} \end{pmatrix}. \quad (14)$$

The L eigenvalues of (14), taken in absolute value, are precisely the ν_l ’s. The right panel of figure 3 of the paper has been obtained by numerical diagonalization of (14) for $L = 10$.

Infinite subsystem

The double-scaling limit $L \rightarrow \infty$ has been considered in detail in [23–25], where a matrix Riemann-Hilbert problem was solved to determine the asymptotic behavior of the correlation matrix “eigenvalues”. These were used to expressed

the Renyi entropies in terms of elliptic functions and to calculate the spectrum of the reduced density matrix, including the degeneracies of the eigenvalues. Let us start by recollecting

$$S_\alpha = \frac{1}{6} \frac{\alpha}{1-\alpha} \ln(k k') + \frac{1}{3} \frac{1}{1-\alpha} \ln \left(\frac{\theta_3^2(0|\alpha i \tau_0)}{\theta_2(0|\alpha i \tau_0) \theta_4(0|\alpha i \tau_0)} \right) + \frac{1}{3} \ln 2, \quad (15)$$

for $h > 1$ and

$$S_\alpha = \frac{1}{6} \frac{\alpha}{1-\alpha} \ln \left(\frac{k'}{k^2} \right) + \frac{1}{3} \frac{1}{1-\alpha} \ln \left(\frac{\theta_2^2(0|\alpha i \tau_0)}{\theta_3(0|\alpha i \tau_0) \theta_4(0|\alpha i \tau_0)} \right) + \frac{1}{3} \ln 2, \quad (16)$$

for $h < 1$; where

$$\tau_0 \equiv \frac{I(k')}{I(k)}, \quad k' = \sqrt{1-k^2}, \quad (17)$$

$I(k)$ is the complete elliptic integral of the first kind,

$$I(k) = \int_0^1 \frac{dx}{\sqrt{(1-x^2)(1-k^2x^2)}} \quad (18)$$

and the elliptic theta functions are defined as

$$\theta_1(z|\tau) = i \sum_{n=-\infty}^{\infty} (-1)^n e^{i\pi\tau(\frac{2n-1}{2})^2} e^{2iz(n-\frac{1}{2})}, \quad (19)$$

$$\theta_2(z|\tau) = \sum_{n=-\infty}^{\infty} e^{i\pi\tau(\frac{2n-1}{2})^2} e^{2iz(n-\frac{1}{2})}, \quad (20)$$

$$\theta_3(z|\tau) = \sum_{n=-\infty}^{\infty} e^{i\pi\tau n^2} e^{2izn} \quad (21)$$

$$\theta_4(z|\tau) = \sum_{n=-\infty}^{\infty} (-1)^n e^{i\pi\tau n^2} e^{2izn}. \quad (22)$$

The elliptic parameter k collects the information on the microscopics of the model. In [23–25] the anisotropic XY chain was considered. For the Ising case, we have:

$$k = \begin{cases} h, & h < 1, \\ \frac{1}{h}, & h > 1 \end{cases} \quad (23)$$

Eigenvalue behavior

Before we proceed with the calculation of the derivative of the Renyi entropies, we can use the results of [25] to familiarize ourselves with the behavior of the eigenvalues of the reduced density matrix obtained by tracing out half of an infinite chain. In [25], it was showed that these eigenvalues are given by an exact geometric sequence, with known degeneracies which do not depend on the parameters of the model (within a given phase) and which have an interesting number-theoretical interpretation. Here we present some simple, qualitative considerations: a careful analysis of the behavior of the

some of these results.

The analytical expressions for the Renyi entropies of the XY chain were derived in [24] and they can be written as

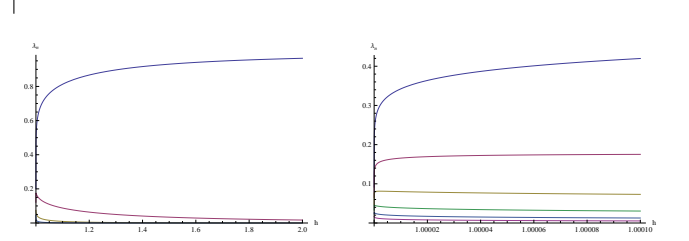


FIG. 7. Case $h > 1$: Plot of the first few eigenvalues of the reduced density matrix in the bipartite thermodynamic limit, as given by (24). The highest eigenvalue is unique, the second is doubly degenerate and so forth. The plot on the right displays a blow-out close to the phase transition and shows that, except for the first, each eigenvalue grows as one moves closer to $h \rightarrow 1$ until it reaches a maximum and starts decreasing to zero. The smaller the eigenvalues, the closer to $h = 1$ this maximum is reached.

eigenvalues in relation to local convertibility will be a subject of a sequent paper.

Case 2 ($h > 1$): “paramagnetic” phase

The eigenvalues of the reduced density matrix ρ_A in the bipartite thermodynamic limit are given by

$$\lambda_n = e^{\frac{1}{6} \ln \frac{k k'}{4} - \pi \frac{I(k')}{I(k)} [n - \frac{1}{12}]}, \quad n = 0, 1, 2, \dots \quad (24)$$

Thus, traces of powers of ρ_A can be written as

$$\text{Tr } \rho_A^\alpha = \sum_{n=0}^{\infty} a_n \lambda_n^\alpha, \quad \lambda_n = e^{-\pi\tau_0 n + \frac{\pi\tau_0}{12} + \frac{1}{6} \ln \frac{k k'}{4}}, \quad (25)$$

with the first few multiplicities being $a_0 = 1, a_1 = 2, a_2 = 1, a_3 = 2, a_4 = 4, \dots$

We show in figure 7 a plot of the first few eigenvalues as a function of h . The highest λ_1 tends to saturate to unity at high magnetic field and decreases monotonically to zero, slowly at first and then progressively faster closer to the phase transition. The other eigenvalues λ_n start at 0 at $h \rightarrow \infty$ and then grow toward a maximum as the magnetic field is lowered. This maximum is reached progressively (exponentially) closer to $h = 1$ for higher n , before each eigenvalue inverts its trend and starts decreasing toward 0.

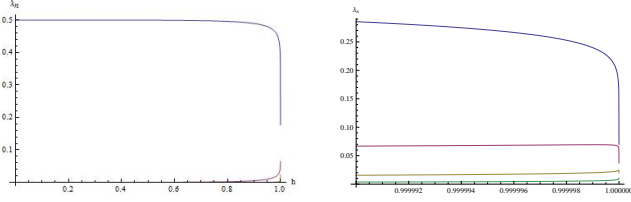


FIG. 8. Case $h < 1$: Plot of the first few eigenvalues of the reduced density matrix in the bipartite thermodynamic limit, as given by (26), degeneracies not shown. In this phase, the highest eigenvalue is doubly degenerate, and all the others have higher (even) multiplicities. The plot on the right displays a blow-out close to the phase transition and shows again the non-monotonous behavior of the eigenvalues we observed in the paramagnetic phase, with the exception of the first, which is always decreasing.

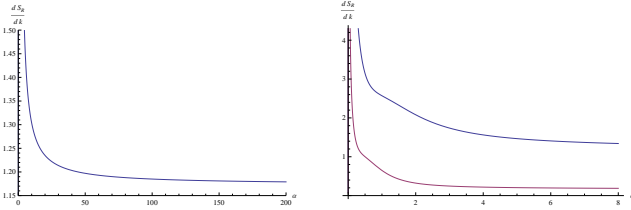


FIG. 9. Case $h > 1$: Plot of the derivative of the α -Renyi entropy with respect to the elliptic parameter as a function of α , according to (36). On the left, the plot at $h = 1.1$, on the right, for a smaller range of α , the plot for $h = 1.1$ (upper curve) and $h = 2$ (lower curve).

Case 1 ($h < 1$): “ferromagnetic” phase

In the ferromagnetic phase the eigenvalues of ρ_A can be written as

$$\lambda_n = e^{\frac{1}{6} \ln \frac{k'}{4k^2} - 2\pi \frac{I(k')}{I(k)} [n + \frac{1}{12}]}, \quad n = 0, 1, 2, \dots \quad (26)$$

and thus

$$\text{tr} \rho_A^\alpha = \sum_{n=0}^{\infty} b_n \lambda_n^\alpha, \quad \lambda_n = e^{-2\pi \tau_0 n - \frac{\pi \tau_0}{6} + \frac{1}{6} \ln \frac{k'}{4k^2}}. \quad (27)$$

The first few degeneracies are $b_0 = 2, b_1 = 4, b_2 = 6, b_3 = 8, \dots$. Most noticeably (and contrary to what observed for small partitions), the highest eigenvalue is always (exactly) doubly degenerate.

We plot the first few eigenvalues as a function of the magnetic field in figure 8. Qualitatively, the behavior is similar to that of figure 7, but with $h \rightarrow 1/h$. However, this time the

highest eigenvalue saturates at 0.5 at $h = 0$, due to its double multiplicity.

Derivative of the entropy

In adherence to the notations of [24, 25], we shall first calculate the derivative of the entropy with respect to the elliptic parameter k , eq. (23). Two identities are important for the

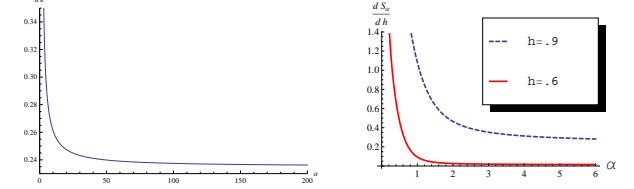


FIG. 10. Case $h < 1$: Plot of the derivative of the α -Renyi entropy with respect to the elliptic parameter as a function of α , according to (38). On the left, the plot for $h = .9$, on the right, for a smaller range of α , the plot again at $h = 0.9$ (upper curve) and $h = .6$ (lower curve).

following derivations:

$$\frac{dI(k)}{dk} = \frac{E(k)}{kk'^2} - \frac{I(k)}{k}, \quad (28)$$

$$\frac{dI(k')}{dk'} = \frac{E(k')}{k'k^2} - \frac{I(k')}{k'}, \quad (29)$$

$$[E(k) - I(k)] I(k') = \frac{\pi}{2} - E(k') I(k), \quad (30)$$

where

$$E(k) \equiv \int_0^1 \sqrt{\frac{1-k^2x^2}{1-x^2}} dx \quad (31)$$

is the complete elliptic integral of the second type.

Combining these identities, we have

$$\frac{dI(k')}{dk} = \frac{dk'}{dk} \frac{dI(k')}{dk'} = -\frac{E(k')}{kk'^2} + \frac{kI(k')}{k'^2}, \quad (32)$$

$$\frac{d\tau_0}{dk} = \frac{d}{dk} \frac{I(k')}{I(k)} = -\frac{\pi}{2} \frac{1}{kk'^2} \frac{1}{I^2(k)}. \quad (33)$$

Since (15, 16) are not in the most suitable form to study their derivatives, we will use the equivalent expressions given in [24]:

$$S_R(\rho_A, \alpha) = \begin{cases} \frac{1}{12} \frac{\alpha}{1-\alpha} \ln \left(\frac{k^2 k'^2}{16q} \right) + \frac{2}{1-\alpha} \sum_{m=0}^{\infty} \ln [1 + q^{(2m+1)\alpha}] & h > 1 \\ \frac{1}{6} \frac{\alpha}{1-\alpha} \ln \left(\frac{16qk'}{k^2} \right) + \frac{2}{1-\alpha} \sum_{m=1}^{\infty} \ln [1 + q^{2m\alpha}] + \ln 2 & h < 1 \end{cases}, \quad (34)$$

where

$$q \equiv e^{-\pi \tau_0} = e^{-\pi I(k')/I(k)}. \quad (35)$$

Case 2 ($h > 1$): “paramagnetic” phase

Having set this ground work, it is now straightforward to compute the derivative of the Renyi entropy by the elliptic

parameter:

$$\frac{dS_R(\rho_A, \alpha)}{dk} = \frac{\alpha}{1-\alpha} \frac{1}{24I^2(k)} \frac{1}{kk'^2} \left[4I^2(k)(1-2k^2) - \pi^2 + 24\pi^2 \sum_{m=0}^{\infty} \frac{2m+1}{q^{-(2m+1)\alpha} + 1} \right] \quad (36)$$

We plot this expression as a function of α in fig. 9, which shows that it is always positive.

In this phase, we have $\frac{dk}{dh} = -\frac{1}{h^2}$ and thus

$$\frac{dS_R}{dh} = -\frac{1}{h^2} \frac{dS_R}{dk}. \quad (37)$$

Hence, the entropy is monotonously decreasing as h increases.

Case 1 ($h < 1$): “ferromagnetic” phase

In this phase we have

$$\frac{dS_R(\rho_A, \alpha)}{dk} = \frac{\alpha}{1-\alpha} \frac{1}{12I^2(k)} \frac{1}{kk'^2} \left[2I^2(k)(k^2-2) + \pi^2 + 24\pi^2 \sum_{m=1}^{\infty} \frac{m}{q^{-2m\alpha} + 1} \right] \quad (38)$$

Figure 10 shows the behavior of this expression as function of α and it is clear that it is qualitatively very similar to that of the paramagnetic phase.

However, since $\frac{dk}{dh} = 1$ in this phase,

$$\frac{dS_R}{dh} = \frac{dS_R}{dk}. \quad (39)$$

Once again, the entropy is monotonous everywhere and there is no sign change of the entropy derivative as a function of α , showing a qualitatively different behavior compared to the small partitions case.

Qualitative analysis

Finally, let us confirm our understanding, by looking at the behavior of the entropy derivative in the $\alpha \rightarrow \infty$ and $\alpha \rightarrow 0$ limits.

$$\alpha \rightarrow \infty$$

This limit can be taken directly from (36) and (38), giving to highest order:

$$\frac{dS_R(\rho_A, \alpha)}{dk} \underset{\alpha \rightarrow \infty}{\simeq} -\frac{1}{24I^2(k)} \frac{1}{kk'^2} \begin{cases} \left[4I^2(k)(1-2k^2) - \pi^2 \right] & h > 1 \\ \left[2I^2(k)(k^2-2) + \pi^2 \right] & h < 1 \end{cases} \quad (40)$$

It is easy to see that the quantities in square brackets are always negative and thus that the entropy derivative is always positive for any k . Moreover, since

$$I(k) \xrightarrow{k \rightarrow 0} \frac{\pi}{2}, \quad I(k) \xrightarrow{k \rightarrow 1} \infty, \quad (41)$$

the entropy derivative for $\alpha \rightarrow \infty$ diverges for $k \rightarrow 1$ and tends to zero from above for $k \rightarrow 0$.

$$\alpha \rightarrow 0$$

This limit cannot be taken directly, since the elements of the series tend to become comparable as α becomes smaller. Thus, we need to first perform a modular transformation on the elliptic theta functions in (15, 16):

$$\frac{\theta_3^2(0|\alpha i\tau_0)}{\theta_2(0|\alpha i\tau_0) \theta_4(0|\alpha i\tau_0)} = \frac{\theta_3^2\left(0\left|-\frac{1}{\alpha i\tau_0}\right.\right)}{\theta_2\left(0\left|-\frac{1}{\alpha i\tau_0}\right.\right) \theta_4\left(0\left|-\frac{1}{\alpha i\tau_0}\right.\right)} = \frac{1}{2} \tilde{q}^{-1/4} \prod_{n=0}^{\infty} (1 + \tilde{q}^{2n+1})^6, \quad (42)$$

$$\frac{\theta_2^2(0|\alpha i\tau_0)}{\theta_3(0|\alpha i\tau_0) \theta_4(0|\alpha i\tau_0)} = \frac{\theta_2^2\left(0\left|-\frac{1}{\alpha i\tau_0}\right.\right)}{\theta_3\left(0\left|-\frac{1}{\alpha i\tau_0}\right.\right) \theta_4\left(0\left|-\frac{1}{\alpha i\tau_0}\right.\right)} = \frac{1}{2} \tilde{q}^{-1/4} \prod_{n=0}^{\infty} (1 - \tilde{q}^{2n+1})^6, \quad (43)$$

where

$$\tilde{q} \equiv e^{-\pi/(\alpha\tau_0)} = e^{-\frac{\pi I(k)}{\alpha I(k')}}. \quad (44)$$

Inserting this into (15, 16) we get

$$S_R(\rho_A, \alpha) = \begin{cases} \frac{1}{6} \frac{\alpha}{1-\alpha} \ln \frac{kk'}{4} + \frac{1}{\alpha(1-\alpha)} \frac{\pi}{12\tau_0} + \frac{2}{1-\alpha} \sum_{m=0}^{\infty} \ln[1 + \tilde{q}^{2m+1}] & h > 1 \\ \frac{1}{6} \frac{\alpha}{1-\alpha} \ln \frac{k'}{4k^2} + \frac{1}{\alpha(1-\alpha)} \frac{\pi}{12\tau_0} + \frac{2}{1-\alpha} \sum_{m=0}^{\infty} \ln[1 - \tilde{q}^{2m+1}] & h < 1 \end{cases} \quad (45)$$

Taking the derivative with respect to the elliptic parameter, we get

$$\begin{aligned} \frac{dS_R(\rho_A, \alpha)}{d\alpha} &= \frac{1}{\alpha(1-\alpha)} \frac{1}{24I^2(k')} \frac{1}{kk'^2} \times \\ &\times \left[\pi^2 - 24\pi^2 \sum_{m=0}^{\infty} \frac{2m+1}{\tilde{q}^{-(2m+1)} + 1} + 4\alpha^2 I^2(k') (1 - 2k^2) \right] \end{aligned} \quad (46)$$

for $h > 1$ and

$$\begin{aligned} \frac{dS_R(\rho_A, \alpha)}{d\alpha} &= \frac{1}{\alpha(1-\alpha)} \frac{1}{24I^2(k')} \frac{1}{kk'^2} \times \\ &\times \left[\pi^2 + 24\pi^2 \sum_{m=0}^{\infty} \frac{2m+1}{\tilde{q}^{-(2m+1)} - 1} + 4\alpha^2 I^2(k') (k^2 - 2) \right] \end{aligned} \quad (47)$$

for $h < 1$.

It is evident that both expressions diverge to positive infinity as $\alpha \rightarrow 0$.

Numerical results of thermal ground states

Here we display the numerical results of the thermal ground state of $N=200$ systems with different bipartitions. From Fig. 11 we can see that the differential local convertibility of subsystem size larger the length scale differs significantly from those smaller than the length scale.

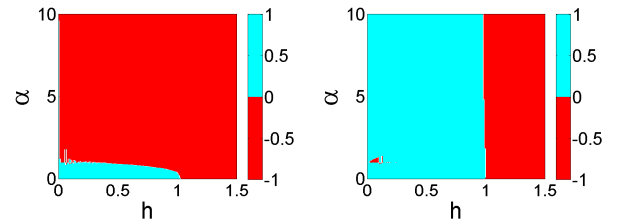


FIG. 11. (Color online) Numeric results of differential local convertibility for the ferromagnetic (thermal ground) state. On the left, a partition $200 = 99|2|99$, which agrees very well with the analytical results in Fig. 4, on the right $200 = 50|100|50$.

* fabiof@mit.edu, hfan@iphy.ac.cn

- [1] L. Amico, R. Fazio, A. Osterloh, and V. Vedral, *Rev. Mod. Phys.* **80**, 517 (2008).
- [2] J. Eisert, M. Cramer, and M. B. Plenio, *Rev. Mod. Phys.* **82**, 277 (2010).
- [3] Z.-G. Gu and X.G. Wen, *Phys. Rev. B* **80**, 155131 (2009)
- [4] Lloyd S. Universal Quantum Simulators, *Science* **273**, 1073 (1996).

- [5] E. Farhi et al, *Science* **292**, 472 (2001).
- [6] Itan Barmes, Stefan Witte, Kjeld S.E. Eikema. *Nature Photonics* **7**, 38(2013); Ronald Hanson and David D. Awschalom, *Nature* **453**, 1043 (2008).
- [7] M. D. Lukin and P. R. Hemmer. *Phys. Rev. Lett.* **84**, 2818 (2000).
- [8] E. Knill, R. Laflamme, R. Martinez and C.-H. Tseng *Nature* **404**, 368 (2000).
- [9] Cui, J., Gu, M., Kwek, L. C., Santos, M. F., Fan, H. & Vedral, V. Quantum phases with differing computational power. *Nature Commun.* **3**, 812 (2012).

- [10] Cui, J., Amico, L., Fan, H., Gu, M., Hamma, A. & Vedral, V. Local characterization of 1d topologically ordered states. Preprint at *arXiv*:1304.2279 (2013).
- [11] Hamma, A., Cincio, L., Santra, S., Zanardi, P., & Amico, L. Local response of topological order to an external perturbation. *Phys. Rev. Lett.* **110**, 210602 (2013).
- [12] Nielsen, M. A. Conditions for a class of entanglement transformations. *Phys. Rev. Lett.* **83**, 436 (1999).
- [13] Jonathan, D. & Plenio, M. B. Entanglement-assisted local manipulation of pure quantum states. *Phys. Rev. Lett.* **83**, 3566 (1999).
- [14] Turgut, S. Catalytic transformations for bipartite pure states. *J. Phys. A: Math. Theor.* **40**, 12185 (2007).
- [15] Klimesh, M. Inequalities that collectively completely characterize the catalytic majorization relation. Preprint at *arXiv*:0709.3680 (2007).
- [16] Lieb E., Schultz T., & Mattis D. Two Soluble Models of an Antiferromagnetic Chain. *Ann. of Phys.* **16**, 407 (1961).
- [17] Kitaev A. Unpaired Majorana fermions in quantum wires. Preprint at *arXiv*: cond-mat/0010440 (2000).
- [18] Chung M.-C., & Peschel I., Density-Matrix Spectra of Solvable Fermionic Systems. *Phys. Rev. B* **64**, 064412 (2001).
- [19] Peschel I. Calculation of reduced density matrices from correlation functions. *J. Phys. A: Math. Gen.* **36** L205 (2003).
- [20] Vidal G., Latorre J. I., Rico E., & Kitaev A. Entanglement in quantum critical phenomena. *Phys. Rev. Lett.* **90**, 227902 (2003).
- [21] Latorre J. I., Rico E., & Vidal G. Ground state entanglement in quantum spin chains. *Quant. Inf. Comput.* **4**, 48 (2004).
- [22] Nielsen M.A., & Chuang I.L., Quantum computation and quantum information. *Cambridge University Press* (2004).
- [23] Its A.R., Jin B.-Q., Korepin V. E., *J. Phys. A* **38**, 2975 (2005).
- [24] Franchini F. , Its A. R., & Korepin V. E. Renyi Entropy of the XY Spin Chain. *J. Phys. A: Math. Theor.* **41**, 25302 (2008).
- [25] Franchini F., Its A.R. , Korepin V.E., & Takhtajan L.A. Entanglement Spectrum for the XY Model in One Dimension. *Quantum Inf. Proc.* **10**, 325 (2011) .
- [26] Feynman R.P. Simulating Physics with Computers. *Int. J. Th. Phys.* **21**, 467 (1982).